strain
An International Journal for Experimental Mechanics

Mechanical Characterisation of Metals by Indentation Tests: An Experimental Verification Study for On-site Applications

G. Bolzon*, B. Molinas† and M. Talassi*

*Department of Structural Engineering, Politecnico di Milano, Piazza Leonardo da Vinci 32, 20133 Milano, Italy
†Venezia Tecnologie S.p.A., Via delle Industrie 39, 30175 Porto Marghera, Venezia, Italy

ABSTRACT: Mechanical characterisation techniques have been recently proposed, which use as main information source the geometry of the residual imprint left on metal surfaces by hardness or instrumented indentation tests. Relevant identification procedures have been developed but the problem has been investigated, so far, mainly from a methodological point of view, exploiting pseudo-experimental data. This contribution presents the results of a verification study based on the real deformation measurements, collected from tests performed at scales consistent with those of structural applications. It is shown that the recovered mechanical properties compare satisfactorily well with those resulting from traditional tensile tests.

KEY WORDS: *constitutive response, experimental verification, indentation test, metals, non-destructive techniques*

Introduction

A spreading approach to the mechanical characterisation of several materials is based on the instrumented indentation, which represents the quite natural evolution of the classical hardness test. During the experiment, a controlled load is applied on the surface of the investigated sample by a tip of pre-fixed shape. The magnitude of the force is continuously monitored together with the corresponding tip penetration depth. This information returns the so-called indentation curves, which are exploited in a growing number of parameter identification procedures based either on popular semi-empirical formulae [1, 2] or on more sophisticated inverse analysis tools [3–18].

Questions have been risen about the reliability of the material properties identified on the basis of the indentation curves only. In some circumstances, in fact, several parameter sets can approximate the same experimental output to the same extent [8, 19]. This lack of identifiability has been partly circumvented by considering the geometry of the residual imprint left on the material surface after the test as additional information source to be exploited to parameter calibration purposes [9, 20, 21].

Instrumented indentation is often performed at the submicron scale [22–25], where alternative testing techniques are hardly applicable. Thus, most equipment available on the market work on the range of a few N maximum force (see e.g. [23] for a non-exhaustive list of typical equipment characteristics), and topological data are recovered by means of atomic force microscopes, as documented in Ref. [20]. However, the test has been recently conceived also for the application at macroscopic scale, with maximum load of the order of some tenths to a few kN [14, 17, 18, 26, 27], typical of classical hardness measurement of metals for structural applications [28–30].

Low amplitude loads permit to control the equipment deformation with contrast frames of reduced dimensions, an important issue for portable instruments and *in situ* applications. On the other hand, reducing the applied loads reduces the size of the sampled material volume and amplifies the effect of imperfection of the indenter tip geometry and of surface finishing. Thus, the experimental output may not be as reliable as desired.

This article presents the results of a mechanical characterisation study concerning metal specimens subjected to hardness or instrumented indentation tests performed at load levels conforming to existing Standards for structural applications [28–30]. Differently from most available literature, experimental information has been collected both from the indentation curves, when available, and from the geometry of the residual imprints. These data have been exploited either jointly or separately, to evaluate the robustness, the accuracy and the reliability of identification procedures based on one information source only. The final goal is to assess the potentialities of inverse analysis techniques that may be exploited for non-destructive diagnosis of structural components on site, where the acquisition of some data may be prevented, for example, by the equipment encumbrance.

The inverse analysis methodology exploited for the present identification purposes has been thoroughly verified in a systematic preliminary work on simulated experiments, where modelling errors are ruled out [9, 21, 31, 32]. The present contribution is intended to evidence the effectiveness of this approach in the case of common (commercial, not model) materials, an important issue for practical applications.

The results reported in this article concern real tests performed on low hardening materials like ingot electrolytic copper and pipeline steel, which exhibit piling-up and do not allow to rely on popular semi-empirical formulae, developed for instance by Oliver and Pharr [1, 2] for the evaluation of the elastic moduli, mainly for the difficulty of estimating the actual contact surface [9, 10, 33].

This investigation has been carried out at Venezia Tecnologie laboratories (shortly: Vetec, Venezia, Italy) and at the Politecnico di Milano (Polimi, Milano, Italy). Material samples have been selected and subjected to tensile and indentation tests at Vetec. To avoid any biased conclusion,

doi: 10.1111/j.1475-1305.2012.00850.x

the only rough indentation output has been initially transferred to Polimi, where the inverse analysis procedures summarised in this article have been applied to recover the material properties, finally compared with those gathered from the tensile tests performed at Vetec.

The mechanical response of the investigated metals has been described by Huber–Hencky–von Mises elastic–plastic constitutive model with isotropic exponential hardening. The relevant parameters to be recovered by inverse analysis consist of the elastic modulus, the initial yield limit and a hardening coefficient, which can be indicative of undergoing degradation phenomena [34]. More sophisticated constitutive relationships can better represent details of the material response but involve a larger number of material parameters and more elaborated testing and identification procedures, which can be performed in laboratory but are hardly transferable to on-site applications. This is particularly the case of the viscous effects considered for instance in Refs. [13, 14], which are more sensitive to environmental conditions (e.g. temperature) than other mechanical properties.

Indentation Results

The aim of this work is to verify the possibility of obtaining reliable information about the mechanical characteristics of metals for long-life monitoring and diagnosis of structural components exploiting the output of classical hardness tests, supplemented by the mapping of the imprint left on the metal surface, which can be recovered by portable equipment nowadays available on the market.

This study considers the possibility that data concerning the controlled penetration depth of the indenter tip versus the applied load may not be available from on-site investigation, because of the encumbrance of the necessarily stiff contrast frame of instrumented indenters.

The loads envisaged for practical applications are of the order of a few kN, consistent with the specifications provided by the Standards [28–30], but some preliminary exploration has been performed for comparative purposes with a universal hardness tester (Zwick/Roell ZHU 0,2, Zwick Roell, Ulm - Einsingen, Germany), applying 200 N maximum load, as in the investigations documented in Refs. [14, 17, 18, 25]. An electrolytic copper ingot and steel extracted from a pipeline are the present reference materials.

Copper slices ($70 \times 70 \times 9$ mm^3) have been cut from the ingot. Surfaces to be indented have been subjected to lapping and polishing procedure, which reduced the surface roughness parameter Ra to 0.16 μm (0.19 μm Rq). The material presents a relative large microstructure, with about 60 μm average grain size determined according to ASTM E112 – 10 Standard [35].

The grain size of the main components (ferrite and perlite) of the considered steel ranges between 10 and 20 μm; some perlite and bainite phases present grains of 30 μm maximum size. These are typical values of alloys for industrial purposes without special laboratory treatments (like grain growth, recrystallisation or second recrystallisation). Lapping and polishing procedure produced the surface roughness Ra equal to 0.26 μm (0.37 μm Rq).

Specimens cut from the copper ingot have been subjected to preliminary indentation tests performed under controlled maximum penetration speed (150 μm min^{-1}) up to the maximum load (200 N) allowed by the laboratory instrument Zwick/Roell ZHU 0,2 equipped with both spherical and conical tip to select the best experimental setup. The corresponding indentation curves are represented in Figure 1. It is worth noticing that the results generated by the spherical tip are more dispersed than those gathered from the conical one. Likely, the larger penetration depth produced by the cone for any applied force makes the sampled volume more representative of the overall material behaviour and the response almost independent of surface effects and local imperfections. All remaining tests were performed, then, by conical tips conforming to Rockwell Standards [29, 30].

The precision achievable by deformation measurements has been initially assessed on the imprints left on copper by Rockwell (grade C) hardness tests (1470 N applied maximum load), considering the accurate mapping produced by a contact profilometer (Zeiss TSK Surfcom 1800 D, Carl Zeiss AG, Oberkochen, Germany) in a metrology centre. Rough data relevant to a typical imprint are graphically represented in Figure 2(A); these have been processed and referred to a local reference system defined as follows: one reference plane is assumed to coincide with the undisturbed flat surface lying far from the indented area; the origin of the local reference system is located on the intersection of the undisturbed plane with a line orthogonal to it, passing through the bottom point of the imprint; this latter line is assumed to coincide with the symmetry axis of the geometry produced by the indentation test. The imprint profiles along 8 radial directions (rotated of 45°

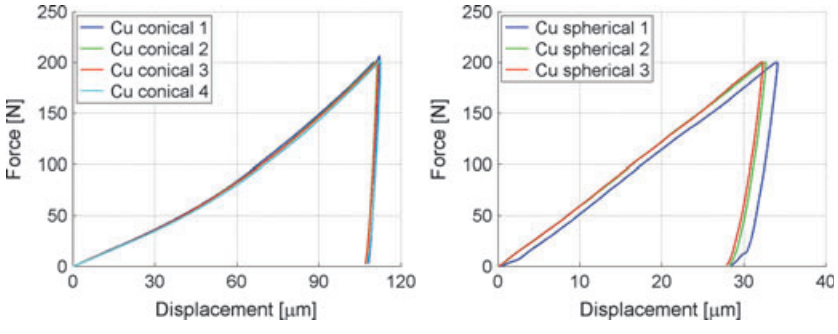

Figure 1: Indentation curves returned by conical (left) and spherical (right) tip on copper specimens by a laboratory universal hardness tester (Zwick/Roell ZHU 0,2)

doi: 10.1111/j.1475-1305.2012.00850.x

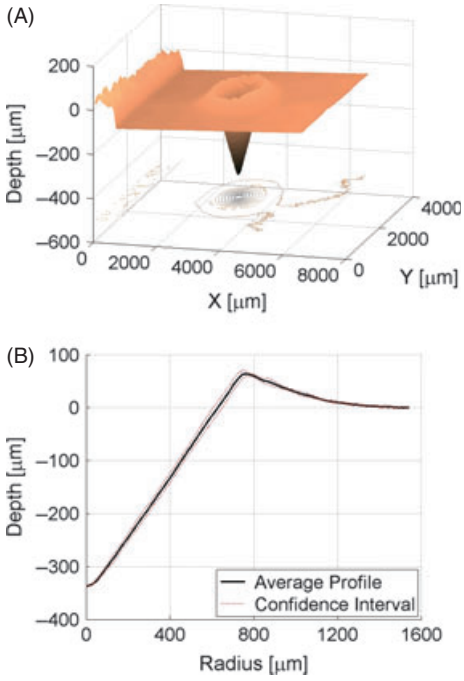

Figure 2: Residual imprint left by a Rockwell hardness tester (Wolpert W Testor) on copper: rough data (A) and mean profile (B) returned by a contact profilometer (Zeiss TSK Surfcom 1800 D) in the laboratory of a metrology centre

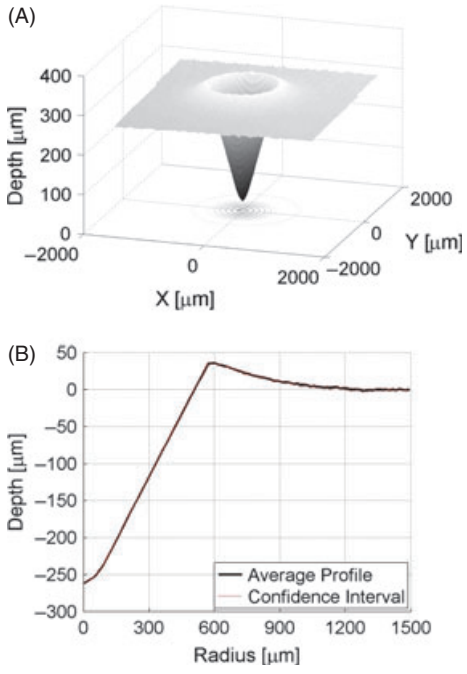

Figure 3: Residual imprint left by a Rockwell hardness tester on pipeline steel: rough data (A) and mean profile (B) returned by a portable equipment with optical detection of the surface topography

each from the other) are considered, and the out-of-reference-plane coordinates of points at corresponding radial distance are averaged.

The mean profile deduced from the graph of Figure 2(A) is reported in Figure 2(B) with the relevant confidence interval. The low observed dispersion reflects both the isotropy of the material response and the reliability of the measurements, which were assumed as target values to assess the performance of available equipment to be eventually used for *in situ* diagnostic analysis.

Figure 3 shows the accurate mapping of the surface topography, which can be recovered by a portable microscope with controlled focal distance. The deformation represented in Figure 3 has been produced by instrumented indentation on the internal surface of a steel pipeline by a portable indenter (Affri SR-HU09-P, Affri, Varese - Induno Olona, Italy). The maximum 2 kN load has been applied in 10 s, hold for further 10 s and then unloaded in 10 s. The corresponding indentation curve (named Z1) is graphed in Figure 4. It is practically superimposed to the curve named Z2, relevant to a test performed in a close position. Worth to be noticed are the repeatability of the experimental results and the fairly good correspondence of the value of the maximum residual displacement left on the material surface at unloading, returned either by the sensing device of the indentation tool (260 μm) or by the geometry mapping (262 μm).

Figure 4 reports also the indentation curves relevant to tests (named Y) performed on the external pipe surface. A larger dispersion and a deeper residual deformation (about 275 μm maximum displacement) are observed in this case.

The experimental information represented in Figures 1–4 (and other similar ones) has been exploited to identification

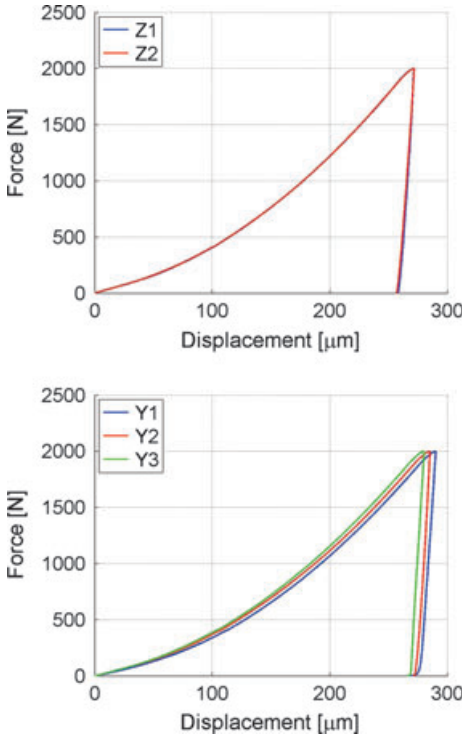

Figure 4: Indentation curves returned by a portable indenter (Affri SR–HU09–P) applied to the internal (Z) and external (Y) surface of a steel pipe

purposes. More specifically, 50 points along both the ascending and the descending branches of the indentation curves have been selected and the corresponding coordinates have been stored for their future use together with the data relevant to the residual deformation. The geometry of the imprint is described by the out-of-reference-plane

doi: 10.1111/j.1475-1305.2012.00850.x

displacements measured at the removal of the indenter tool at 100 equally spaced points situated along the radius of the mean imprint profile, spanning a length equal to 2.5 times the distance from the imprint axis to the position of the maximum piling-up point.

Identification Procedure

The mechanical response of the investigated metals was assumed to be isotropic, obeying the classical Huber–Hencky–von Mises plasticity criterion with exponential hardening rule. This choice represents a reasonable compromise between the accuracy of the modelled material response and the number of the governing parameters, the exiguity of which helps enhancing the robustness of the relevant identification procedures. In particular, viscous effects producing the observed rounding and a small plateau of the indentation curves during the load holding time before unloading were neglected.

Thus, under uniaxial loading, the stress value σ beyond the elastic limit evolves with the corresponding total strain ε according to the relationship:

$$\sigma \equiv \sigma_0 = \sigma_Y \left(\frac{E\,\varepsilon}{\sigma_Y}\right)^n \tag{1}$$

where the elastic modulus E, the initial yield limit σ_Y and the hardening coefficient n are material constants.

This hardening rule can be generalised to multi-axial states assuming that σ and ε coincide with the corresponding equivalent stress and strain measures, namely:

$$\sigma^{eq} = \sqrt{\frac{3}{2}\sigma'_{ij}\sigma'_{ij}}\,, \quad \varepsilon^{eq} = \sqrt{\frac{2}{3}\varepsilon'_{ij}\varepsilon'_{ij}} \tag{2}$$

where σ'_{ij} and ε'_{ij} represent the deviatoric parts of the σ_{ij} and ε_{ij} (respectively) components of Cauchy stress and logarithmic strain tensors.

The evolution of stresses and strains under complex loading conditions is recovered by the following set of constitutive rate (here denoted by a superimposed dot) equations:

$$\dot{\varepsilon}_{ij} = \dot{\varepsilon}^e_{ij} + \dot{\varepsilon}^p_{ij} \tag{3}$$

$$\dot{\varepsilon}^e_{ij} = \frac{1+\nu}{E}\dot{\sigma}'_{ij} + \frac{1-2\nu}{E}\dot{p}\delta_{ij} \tag{4}$$

$$f = \sigma^{eq} - \sigma_0(\varepsilon^{eq}) \tag{5}$$

$$\dot{\varepsilon}^p_{ij} = \dot{\lambda}\frac{\partial f}{\partial \sigma_{ij}} \tag{6}$$

$$f \le 0, \quad \dot{\lambda} \ge 0, \quad f\dot{\lambda} = 0 \tag{7}$$

where strain rates $\dot{\varepsilon}_{ij}$ are decomposed into their elastic $\dot{\varepsilon}^e_{ij}$ and plastic (irreversible) $\dot{\varepsilon}^p_{ij}$ components; p represents the hydrostatic stress associated with the Kronecker delta function δ_{ij}; f indicates the current yield function; and λ denotes the plastic multiplier.

The value of material parameters governing the above relationships can be identified on the basis of the inverse analysis procedures outlined in Ref. [21]. The exploited methodology relies on the comparison of the experimental information gathered from the indentation and the mapping of the imprint with the numerical simulation of the test. The finite element (FE) model developed for the present investigation is visualised in Figure 5. It consists of 2335 nodes and 2164 axis-symmetric 4-node elements. The modelled semi-spherical volume has 5 mm radius; the smallest elements under the indenter tip have 15 μm characteristic size.

The same mesh has been exploited also for some comparative analysis performed on the basis of the preliminary experimental results gathered on copper at 200 N maximum load. In this case, all mesh dimensions have been scaled by factor 5. The discretisation has been chosen as a reasonable compromise between computing time (ranging between 3 and 4 min for each simulation) and result accuracy, after having verified that finer meshes did not enhance significantly the overall output. Boundary conditions satisfy the assumed symmetry along the left side of the mesh

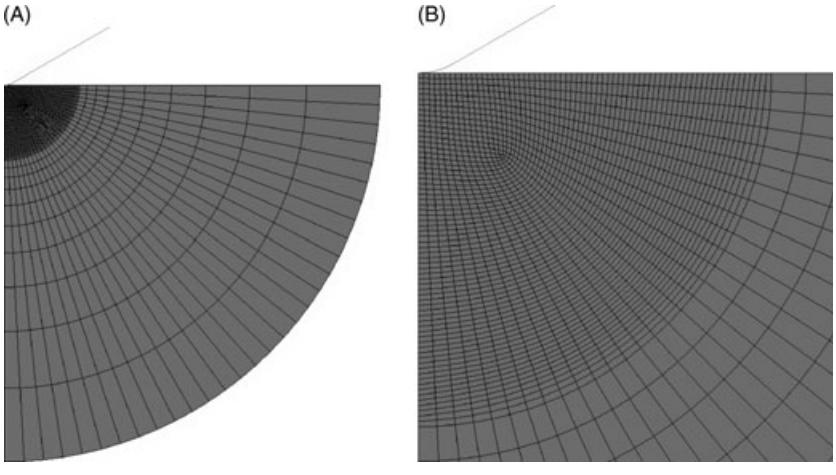

Figure 5: The axis-symmetric finite element model exploited to simulate the indentation test (A) and a zoom of it (B) under the indenter tip, modelled as rigid body

doi: 10.1111/j.1475-1305.2012.00850.x

and constrain all displacements along the circular border, far enough from the indented region to make the results of the overall analysis practically insensitive to this detail.

The considered indenter tip conforms with Rockwell specifications in Standards [29]: sphero-conical geometry with 120° opening angle and rounded spherical end of 200 μm radius. It is made of diamond and, therefore, conceived as a rigid body in the FE model on the basis of previous modelling and computing experience [9, 21]. The interaction between the material sample and the indenter tip obeys Coulomb's relationship with friction coefficient fixed to the realistic value 0.15, account taken of the grade of the commonly performed surface polishing.

Computations are performed by a widely available commercial software [36] in the large strain and large displacement regime, under the hypothesis (reasonable for the investigated processes) that the plastic deformation is much larger than the elastic contribution.

Numerical analyses return the counterparts of the quantities measured in the experiment as a function of the parameters, here collected in vector $\mathbf{z}$, representing the sought material properties, in the present context coinciding with the above introduced elastic modulus E, initial yield limit σ_Y and hardening coefficient n. The alternative semi-empirical formula developed by Oliver and Pharr for the evaluation of the elastic moduli [1, 2] was not exploited to the present purposes as this approach can lead to inaccurate results in the case of piling-up materials, where the determination of the actual contact surface may represent a critical issue [9, 10, 33]. Analogously, the real geometry of Rockwell (sphero-conical) tip considered in the present investigation prevents the use of dimensional analysis, which can be effectively applied to sharp conical indenters, where geometrical similarity is maintained independently of the penetration depth [10, 11].

The optimum parameter values are recovered by the minimisation of a discrepancy function, defined as follows for the present application:

$$\omega(\mathbf{z}) = \alpha \sum_{i=1}^{N_h} \left(\frac{h_{mi} - h_{ci}(\mathbf{z})}{h_{\max}} \right)^2 + \beta \sum_{j=1}^{N_u} \left(\frac{u_{mj} - u_{cj}(\mathbf{z})}{u_{\max}} \right)^2 \qquad (8)$$

In the above relationship, subscripts m and c refer to measured and computed quantities, respectively. In particular, h_{mi} and h_{ci} represent the tip penetration depth for the $N_h = 100$ sampled values of the force applied during the test, at 50 equal incremental steps along both the loading and the unloading branches; u_{mj} and u_{cj} denote the out-of-reference-plane displacement, measured along the profile of the residual imprint at the removal of the load in $N_u = 100$ points mentioned above; $h_{\max}$ and $u_{\max}$ are two normalisation terms, here assumed to coincide with the maximum penetration depth experienced during the test and with the largest residual deformation left on the indented surface; factors α and β assume either 1 or 0 value depending on the source of experimental information to be exploited ($\alpha = 1$ and $\beta = 0$ for the indentation curve alone; $\alpha = 0$ and $\beta = 1$ for the map of the imprint alone; $\alpha = \beta = 1$ when both sources are taken into account).

The minimisation of the discrepancy function (8) can be performed either by a first-order iterative algorithm or by zeroth-order evolutive (genetic) search procedures available in Matlab toolboxes [37].

In this study, exploration by genetic algorithm was made by an initial population of 200 individuals randomly defined within the normalised (by linear scaling in the range between 0 and 1) box-shaped parameter domain; subsequent generations were produced by a large percentage of allowed adaptive feasible mutation while scattered crossover interested only 30% of the population at each generation. The search was arrested when the cumulative change in the fitness function value of all individuals with respect to the former generation is less than the tolerance 10^{-12}. The final result was typically achieved in 150–200 generations. Alternatively, the robust 'trust region' algorithm [38] was used, and the minimum search was performed with termination tolerance 10^{-12} on the function improvement and 10^{-10} on the variation of the normalised parameter values; these targets were usually achieved in 30–40 iterations.

Both optimisation techniques involve heavy computations, since the system response has to be evaluated hundreds to thousands times by the nonlinear FE code, while the only varying input values consist of the constitutive parameters. The computational burden associated with the repetitive simulations required by the general inverse analysis tool developed for the present purposes has been profitably reduced by the implementation of model reduction methodologies based on the proper orthogonal decomposition (or principal component analysis, see [39]) combined with data interpolation techniques. This approach exploits the expected correlation of the numerical results and represents an optimal compromise between opposing requirements: solution accuracy and reliability on one side; reduced computing times, compatible with the routinely use of inverse analysis procedures in industrial environment, on the other. The implemented numerical procedure can be summarised as follows, details can be found in Refs. [31, 41].

A pre-fixed number of numerical analyses is carried out for different combinations of the material properties, collected by vectors $\mathbf{z}_k$. The entries of $\mathbf{z}_k$ are either selected in a regular grid or defined by a random distribution of values in the sought parameter space. The preliminary computations return the penetration depth $h_{ci}(\mathbf{z}_k)$ for given application force and the imprint profiles $u_{cj}(\mathbf{z}_k)$. These *snapshots* (in jargon) are referred to an optimal set of orthonormal reference bases gathered in matrices $\mathbf{\Phi}_h$ and $\mathbf{\Phi}_u$. Each vector in this collection represents a normalised deformation mode associated with indentation. The computed penetration depth and residual deformation can then be expressed as a combination of these elementary contributions, amplified by coefficients stored in matrices $\mathbf{B}_h$, $\mathbf{B}_u$ as follows:

$$\mathbf{h}_c(\mathbf{z}) = \mathbf{\Phi}_h \mathbf{B}_h \mathbf{g}(\|\mathbf{z} - \mathbf{z}_i\|) \qquad \mathbf{u}_c(\mathbf{z}) = \mathbf{\Phi}_u \mathbf{B}_u \mathbf{g}(\|\mathbf{z} - \mathbf{z}_i\|) \qquad (9)$$

Vector $\mathbf{g}$ gathers interpolation functions depending on the Euclidean distance between different points in the

doi: 10.1111/j.1475-1305.2012.00850.x

parameter space $\|\mathbf{z} - \mathbf{z}_i\|$. For the present application, Gauss distributions [40] were selected on the basis of some preliminary numerical computation, so that:

$$g_k(\|\mathbf{z} - \mathbf{z}_k\|) = e^{-\|\mathbf{z}-\mathbf{z}_k\|^2} \quad (10)$$

The analytical model (9) can then be exploited to minimise the discrepancy (8) in real-time computations during the indentation test.

Results

The inverse analysis methodology based on the indentation tests summarised so far has been exploited to recover the constitutive properties of the investigated metal samples. The elastic modulus E, the initial yield limit σ_Y and the hardening coefficient n entering relation (1) represent the parameters (gathered in vector $\mathbf{z}$) to be identified. Poisson's ratio has been fixed in all cases to the common value 0.3, because of the known low sensitivity of indentation results to this parameter [9, 42].

The first validation tests concerned electrolytic copper. Parameter identification has been initially performed on the basis of the information relevant to the indentation curves graphed in Figure 1, obtained at Polimi at the common 200 N maximum load [14, 17, 18, 25]. The gathered values have been compared with those recovered from the geometry of the residual imprint represented in Figure 2, produced by Rockwell C hardness (HRC) test in Vetec laboratories at 1470 N maximum load, which produces a penetration depth of about 300 μm and an imprint of about 800 μm radius, which is thought to be fully representative of the material response on the macroscopic scale despite the relatively large observed microstructure. In this situation, in fact, thousand grains and a relatively large grain boundary area are involved in the test.

The minimum search has been performed by genetic algorithms in the domain specified in Table 1. Reduced models have been trained on the results of 123 successful simulations of the indentation test at 200 N maximum load with input parameter sets defined over a regular $5 \times 5 \times 5$ grid; a few simulations failed because of the excessive deformation of some element of the implemented mesh under the indenter tip for the most ductile material properties. Further 108 successful FE analyses of Rockwell hardness test were performed over the same parameter grid. The discrepancy function (8) has been defined setting $\alpha = 1$ and $\beta = 0$ in the former situation; $\alpha = 0$ and $\beta = 1$ in the latter.

The optimum values of the sought mechanical characteristics for the investigated material samples are listed in Table 2 together with the corresponding nominal tensile strength. The constitutive properties identified in the two inverse analysis exercises are quite different but both sets permit to closely reproduce the relevant indentation responses by FE simulation, see Figure 6. The corresponding reduced model output is also presented, for comparison purposes. Notice that the achieved approximation is quite accurate, despite the relatively low snapshot number.

The parameter values listed in Table 3, obtained from tensile tests carried out according to Standards [43] on the specimens shown in Figure 7, evidence that the mechanical properties of the core material are different from those at the edge of the copper block, likely the most affected by the extrusion process. It is worth to be reported that the specimen direction was hardly distinguishable from the output of most tensile tests, thus confirming the assumed

Table 1: Search domains in the parameter space of the performed inverse analysis exercises

	Elastic modulus E (GPa)	Yield limit σ_Y (MPa)	Hardening exponent n (–)
Electrolytic copper	55–190	100–340	0.01–0.25
Pipeline steel	150–250	200–1000	0.00–0.24

Table 2: Identified constitutive parameters of the electrolytic copper block and corresponding tensile strength (*nominal value)

	Elastic modulus E (GPa)	Yield limit σ_Y (MPa)	Hardening exponent n (–)	Tensile strength (MPa)
Indentation curve – 200 N	185	230	0.017	236*
Residual imprint – Rockwell C hardness test	103	265	0.020	271*

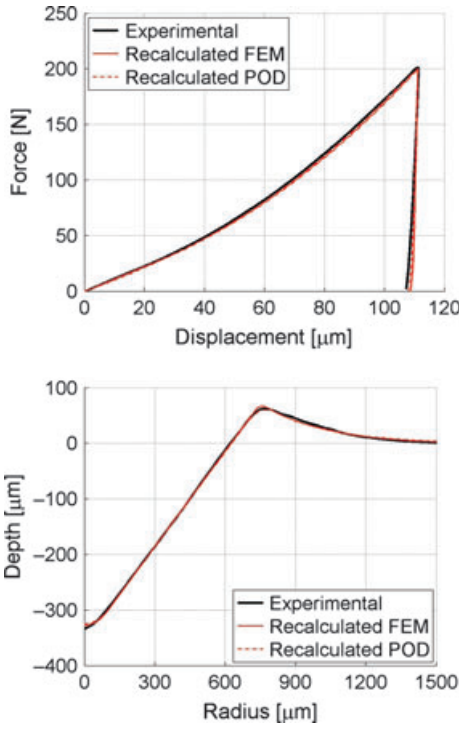

Figure 6: Comparison between the experimental information collected from the indentation of an electrolytic copper block (continuous thick lines) and the corresponding output of the numerical simulation of the tests, performed with identified values of the constitutive parameters by traditional finite element analyses (continuous thin lines) and by the relevant reduced models (dashed thin lines). Notice that the imprint recalculated by the POD–RBF approximation exploited to inverse analysis purposes is practically superimposed to the corresponding experimental result

doi: 10.1111/j.1475-1305.2012.00850.x

Table 3: Constitutive parameters (nominal values) of the electrolytic copper block recovered from the performed uniaxial tensile tests (Figure 8) with the corresponding standard deviation (in brackets, if available)

	Elastic modulus (GPa)	Yield limit (MPa)	Tensile strength (MPa)
Core	103 (±8)	228 (±1)	236 (±1)
Edge	110 (–)	273 (–)	274 (–)

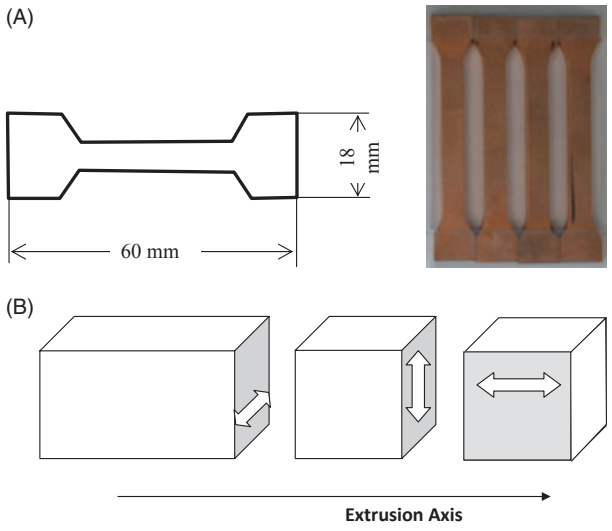

Figure 7: Tensile specimens (A) cut from the copper block along the directions sketched in (B)

material isotropy. Fair correspondence was found in any case with the mechanical response characterised by the parameter sets listed in Table 2. The only meaningful discrepancy concerns the elastic modulus evaluated from the indentation tests performed at 200 N maximum load, which involve a relatively small sampled material volume: about 100 μm maximum penetration depth (versus about 300 μm produced by HRC). Thus, the representativeness of some result may be influenced by the material microstructure, presenting in this case relatively large grain size. However, Figure 8 shows that the overall agreement of the uniaxial curves relevant to copper, obtained either directly from tensile tests or by inverse analysis tools on the basis of the indentation results, is quite satisfactory for structural analysis purposes.

The reduced POD–RBF model concerning instrumented indentation tests performed on steel at 2 kN maximum load has been trained on the output of 700 FE analyses with input parameter sets randomly defined within the range specified in Table 1. Inverse analysis results gathered by genetic algorithm in the case of steel for both the internal (position Z) and external (position Y) pipe surface are reported in Table 4.

The available experimental data are represented in Figures 3 and 4; the average indentation curve has been considered where some dispersion was observed while all imprints were practically identical. Parameters identified on the basis of all available information were recovered

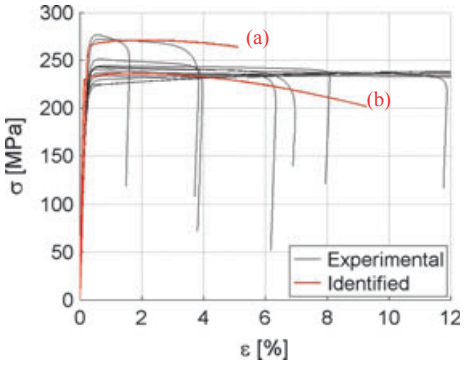

Figure 8: Comparison between the output of uniaxial tests (experimental, thin lines) and the identified response of the investigated electrolytic copper specimens. The constitutive response is represented here in terms of conventional nominal stress and strain values. Curve (a) is identified on the basis of the geometry of the residual imprint left by Rockwell C hardness test on the external ingot surface and compares well with those relevant to tensile tests performed on specimens cut parallel to the extrusion axis close to the ingot edges; curve (b) refers to the experimental information collected from instrumented indentation performed at 200 N maximum applied force in the core material

Table 4: Constitutive parameters of the pipeline steel recovered from indentation test: results recovered by genetic algorithm

	Elastic modulus E (GPa)	Yield limit σ_Y (MPa)	Hardening exponent n (–)	Discrepancy at optimum (–)
Indentation curve only				
Position Z	247	510	0.044	0.0272
Position Y	247	472	0.038	0.0166
Residual imprint only				
Position Z	173	451	0.091	0.0034
Position Y	173	365	0.122	0.0033
Indentation curve and imprint				
Position Z	241	420	0.102	0.0369
Position Y	244	348	0.122	0.0272

setting the same weight $\alpha = \beta = 1$ in the definition of the discrepancy function (8).

In this example, however, the significance of each information source has been also separately evaluated: either the only indentation curve or the only residual imprint has provided input data for the inverse analysis procedures, while the remaining measurements have been exploited for verification purposes, bearing in mind that these data sets may not be available all together in the case of on-site explorations, for example, because of the encumbrance of some equipment.

The inverse analysis exercises have been performed also by a first-order minimisation algorithm, starting from 10 different initialisation vectors randomly selected in the search space defined by the limits listed in Table 1, to overcome the possibility of getting stuck in local minimum points.

The parameters recovered from the information relevant to position Z are listed in Table 5 in terms of: the best matching set, corresponding to the lowest value of the

doi: 10.1111/j.1475-1305.2012.00850.x

Table 5: Identified constitutive parameters of pipeline steel at position Z: discrepancy minimisation by gradient algorithm

	Elastic modulus E (GPa)	Yield limit σ_Y (MPa)	Hardening exponent n (–)
Indentation curve only			
Best matching	247	506	0.047
Mean (SD)	239 (±7)	537 (±27)	0.029 (±0.015)
Residual imprint only			
Best matching	175	450	0.092
Mean* (SD)	193 (±34)	444 (±33)	0.092 (±0.015)
Indentation curve and imprint			
Best matching	241	420	0.102
Mean (SD)	231 (±22)	455 (±73)	0.082 (±0.042)

*Excluding two anomalous outputs.

discrepancy function and practically coinciding with the genetic algorithm output; the average of all realisations returning residual discrepancy values comparable (same order of magnitude) to the best one and then considered admissible in view of the unavoidable experimental and modelling errors. The standard deviation (also reported in Table 5) assesses the reliability of the estimates.

The posterior validation of the identified material properties has been performed by the comparison of experimental and recalculated data. The numerical simulations of the test have been carried out with the best matching parameter sets. Results are visualised in Figures 9 and 10. It is worth noticing that modelling and/or experimental errors are more systematically reflected by the indentation curves rather than by the imprints. In fact, Figure 10 shows that the geometry of the residual profile can be captured almost exactly by the numerical simulation and that a fair agreement is also found with the indentation curves, constituting in this case the verification term. On the contrary, Figure 9 shows that the minimisation procedure based on the indentation curve only does not permit to closely reproduce the residual deformation at unloading. In particular, a quite large discrepancy is observed in the piling-up region of the imprint, which is known to be significantly influenced by the ratio between elastic and plastic properties in low hardening materials [9, 10].

The recalculated results corresponding to the parameter set recovered exploiting the available data all together are compared to the experimental one in Figure 11. Notice the accuracy of the simulated residual imprint.

The best matching parameter sets collected in Table 5 permit to recover the uniaxial material response represented in Figure 12 in terms of nominal stress and strain values. Indeed, a much better agreement is found if the imprint geometry (alone or in combination with the indentation curve) is considered to identification purposes: the overall matching is good and the numerically reconstructed uniaxial curves provide a close upper bound of the relatively disperse results obtained through the tensile test of specimens ($60 \times 18 \times 3$ mm^3) cut from the middle thickness of the pipe.

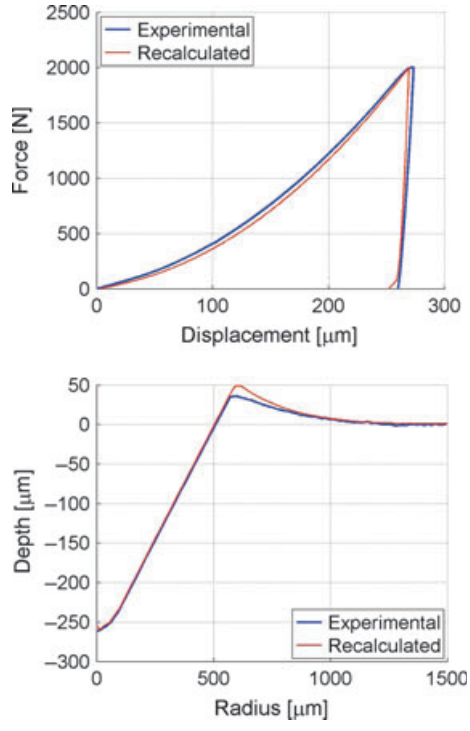

Figure 9: Comparison between the experimental information collected from the indentation of a pipeline steel (position Z) and the corresponding output of the numerical simulation of the test performed with the constitutive parameter values listed in Tables 4 and 5 (best matching set identified on the basis of experimental data concerning the indentation curves only)

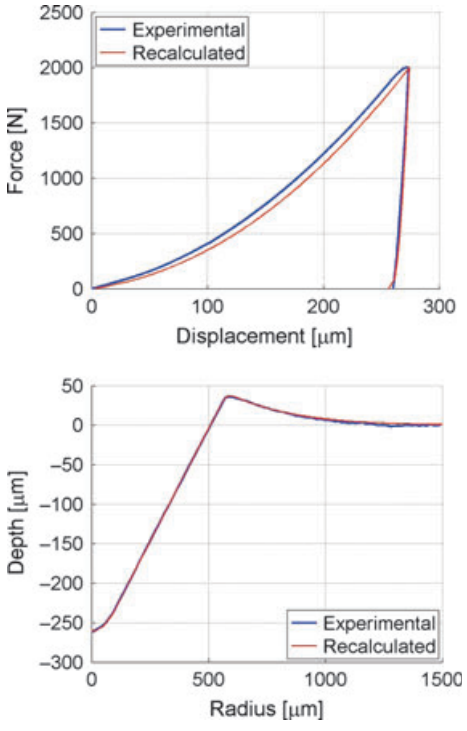

Figure 10: Comparison between the experimental information collected from the indentation of a pipeline steel (position Z) and the corresponding output of the numerical simulation of the test performed with the constitutive parameter values listed in Tables 4 and 5 (best matching set identified on the basis of experimental data concerning the geometry of the residual imprint only)

doi: 10.1111/j.1475-1305.2012.00850.x

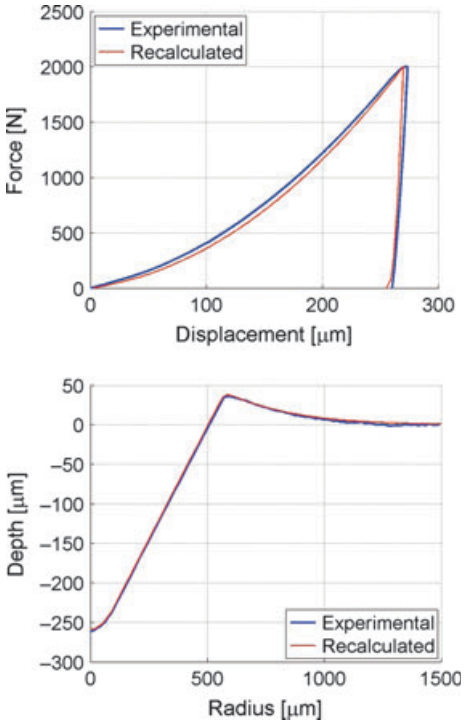

Figure 11: Comparison between the experimental information collected from the indentation of a pipeline steel (position Z) and the corresponding output of the numerical simulation of the test performed with the constitutive parameter values listed in Tables 4 and 5 (best matching set identified on the basis of all available experimental data)

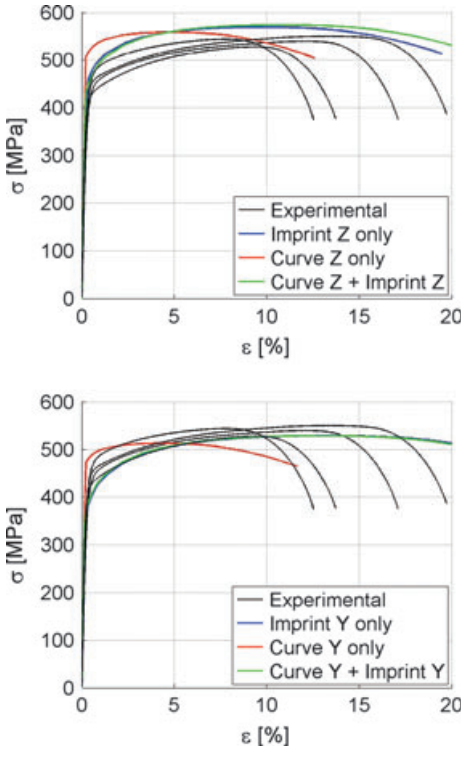

Figure 12: Comparison between the output of uniaxial tests (experimental, thin lines) and the identified response of a pipeline steel, represented in terms of conventional nominal stress and strain values

Table 6: Identified constitutive parameters of pipeline steel at position Y: discrepancy minimisation by gradient algorithm

	Elastic modulus E (GPa)	Yield limit σ_Y (MPa)	Hardening exponent n (–)
Indentation curve only			
Best matching	247	471	0.042
Mean (SD)	238 (±18)	476 (±26)	0.040 (±0.019)
Residual imprint only			
Best matching	173	363	0.123
Mean (SD)	191 (±24)	357 (±8)	0.124 (±0.002)
Indentation curve and imprint			
Best matching	246	351	0.120
Mean (SD)	225 (±20)	359 (±9)	0.120 (±0.012)

Table 7: Constitutive parameters of the pipeline steel recovered from indentation or uniaxial test (nominal values)

	Elastic modulus (GPa)	Yield limit (MPa)	Tensile strength (MPa)
Indentation curve only			
Position Z	239 (±7)	537 (±27)	564 (±4)
Position Y	238 (±18)	476 (±26)	517 (±5)
Residual imprint only			
Position Z	193(±34)	444 (±34)	569 (±1)
Position Y	191 (±24)	357 (±8)	529 (±1)
Indentation curve and imprint			
Position Z	231 (±21)	455 (±73)	577 (±7)
Position Y	225 (±20)	359 (±9)	534 (±3)
Tensile test			
Middle position	191 (±32)	431 (±20)	541 (±9)

The material properties recovered by the gradient algorithm starting from the available experimental information from the external pipeline surface (position Y) are listed in Table 6. Once again, the best matching values correspond to the output of the genetic algorithm.

The simulated uniaxial response is compared in Figure 12 to the output of tensile test in terms of nominal quantities. Quite interestingly, the identified material behaviour at this position represents a close lower bound of the curves returned by the tensile specimens cut from the middle of the pipe. Once more, the consideration of the residual deformation improves the description of the material hardening.

The mechanical characteristics recovered from the different tests performed on the pipe specimen are listed in Table 7. The corresponding standard deviation is also reported (in brackets) when available. The agreement among all values is quite good.

Closing Remarks

A combined experimental–numerical study has been performed with the aim of validating earlier proposed parameter identification procedures, focusing on the

doi: 10.1111/j.1475-1305.2012.00850.x

geometry of the imprint produced by instrumented indentation or traditional hardness test. The main mechanical characteristics (elastic modulus, initial yield limit and hardening coefficient) have been recovered by an inverse analysis tool relying on a simulation model of the experiment. Alternative popular semi-empirical formulae can lead to inaccurate results in the present case of piling-up materials and the actual geometry of the considered Rockwell (sphero-conical) tip prevents the use of dimensional analysis, which can be effectively applied to sharp conical indenters, where similarity is maintained independently of the penetration depth.

The results summarised in this article confirm the great informative content of the residual deformation left on metal surfaces, to be exploited for mechanical characterisation purposes.

In all analysed situations, the consideration of the imprint improved the results of the inverse analysis exercises. The possibility of performing reliable parameter identification from geometrical data only has been also demonstrated, an interesting perspective in view of non-destructive *in situ* diagnostic analysis of metal structures. In fact, easily handling hardness testers are available on the market, and portable mapping equipment that can operate with the required accuracy has been recently produced.

The comparison between corresponding results of truly experimental and numerically simulated indentation tests showed that classical elastic–plastic models interpret quite accurately the mechanical response of metals for structural applications under axis-symmetric stress states. It was further verified that the mechanical properties recovered through standard indentation or hardness tests performed at 1.5–2 kN maximum load are representative of the overall mechanical behaviour of the considered materials, with the indubitable advantages that no specimen extraction is required and that the small tested volumes permit a fine exploration of the spatial distribution of any heterogeneity. Finally, it has been observed that the dispersion of the results recovered from hardness or instrumented indentation test is consistent with that observed in traditional tensile tests.

ACKNOWLEDGEMENTS

This study has been carried out with financial support by Venezia Tecnologie S.p.A., which is gratefully acknowledged. Thanks are due to our Colleagues, G. Maier and D. Giantin, for fruitful preliminary discussions and for the assistance with the laboratory work.

REFERENCES

1. Oliver, W. C. and Pharr, G. M. (1992) An improved techniques for determining hardness elastic modulus using load and displacement sensing indentation experiments. *J. Mater. Res.* **7**, 1564–1583.
2. Oliver, W. C. and Pharr, G. M. (2004) Measurement of hardness and elastic modulus by instrumented indentation: advances in understanding and refinement to methodology. *J. Mater. Res.* **19**, 3–20.
3. Giannakopoulos, A. E. and Suresh, S. (1999) Determination of elastoplastic properties by instrumented sharp indentation. *Scripta Mater.* **40**, 1191–1198.
4. Huber, N. and Tsakmakis, Ch. (1999) Determination of constitutive properties from spherical indentation data using neural networks. *J. Mech. Phys. Solids* **47**, 1569–1607.
5. Venkatesh, T. A., van Vliet, K. J., Giannakopoulos, A. E. and Suresh, S. (2000) Determination of elasto–plastic properties by instrumented sharp indentation: guidelines for property extraction. *Scripta Mater.* **42**, 833–839.
6. Kucharski, S. and Mróz, Z. (2001) Identification of plastic hardening parameters of metals from spherical indentation. *Mater. Sci. Eng. A*, **318**, 65–76.
7. Matsuda, K. (2002) Prediction of stress–strain curves of elastic–plastic materials based on the Vickers indentation. *Philos. Mag. A* **82**, 1941–1951.
8. Capehart, T. W. and Cheng, Y. T. (2003) Determining constitutive models from conical indentation: sensitivity analysis. *J. Mater. Res.* **18**, 827–832.
9. Bolzon, G., Maier, G. and Panico, M. (2004) Material model calibration by indentation, imprint mapping and inverse analysis. *Int. J. Solids Struct.* **41**, 2957–2975.
10. Cheng, Y.-T. and Cheng, C.-M. (2004) Scaling, dimensional analysis, and indentation measurements. *Mater. Sci. Eng. R* **44**, 91–149.
11. Cao, Y. P., Qian, X. Q., Lu, J. and Yao, Z. H. (2005) An energy–based method to extract plastic properties of metal materials from conical indentation tests. *J. Mater. Res.* **20**, 1194–1206.
12. Hernot, X., Bartier, O., Bekouche, Y., El Abdi, R. and Mauvoisin, G. (2006) Influence of penetration depth and mechanical properties on contact radius determination for spherical indentation. *Int. J. Solids Struct.* **43**, 4136–4153.
13. Tyulyukovskiy, E. and Huber, N. (2006) Identification of viscoplastic material parameters from spherical indentation data: part I. Neural networks. *J. Mater. Res.* **21**, 664–676.
14. Klötzer, D., Ullner, C., Tyulyukovskiy, E. and Huber, N. (2006) Identification of viscoplastic material parameters from spherical indentation data: part II. Experimental validation of the method. *J. Mater. Res.* **21**, 677–684.
15. Nakamura, T. and Gu, Y. (2007) Identification of elastic–plastic anisotropic parameters using instrumented indentation and inverse analysis. *Mech. Mater.* **39**, 340–356.
16. Ma, D., Ong, C. W. and Zhang, T. (2009) An instrumented indentation method for Young's modulus measurement with accuracy estimation. *Exp. Mech.* **49**, 719–729.
17. Collin, J.-M., Parenteau, T., Mauvoisin, G. and Pilvin, P. (2009) Material parameters identification using experimental continuous spherical indentation for cyclic hardening. *Comput. Mater. Sci.* **46**, 333–338.
18. Collin, J.-M., Mauvoisin, G. and Pilvin, P. (2010) Materials characterization by instrumented indentation using two different approaches. *Mater. Des.* **31**, 636–640.
19. Chen, X., Ogasawara, N., Zhao, M. and Chiba, N. (2007) On the uniqueness of measuring elastoplastic properties from indentation: the indistinguishable mystical materials. *J. Mech. Phys. Solids* **55**, 1618–1660.
20. Bolzon, G., Bocciarelli, M. and Chiarullo, E. J. (2009) Mechanical characterization of materials by micro-indentation and AFM scanning. In: *Applied Scanning Probe Methods XII Characterization* (B. Bhushan and H. Fuchs, Eds). Springer-Verlag, Heidelberg: 85–120.
21. Bolzon, G., Buljak, V., Maier, G. and Miller, B. (2011) Assessment of elastic-plastic material parameters comparatively by

doi: 10.1111/j.1475-1305.2012.00850.x

three procedures based on indentation test and inverse analysis. *Inverse Probl. Sci. En.* **19**, 815–837.
22. Bhushan, B., Kulkarni, A. V., Bonin, W. and Wyrobek, J. T. (1996) Nanoindentation and picoindentation measurements using a capacitive transducer system in atomic force microscopy. *Philos. Mag. A* **74**, 1117–1128.
23. Bhushan, B. and Li, X. (2003) Nanomechanical characterisation of solid surfaces and thin films. *Int. Mater. Rev.* **48**, 125–164.
24. Stauss, S., Schwaller, P., Bucaille, J. L., Rabe, R., Rohr, L., Michler, J. and Blank, E. (2003) Determining the stress–strain behaviour of small devices by nanoindentation in combination with inverse methods. *Microelectron. Eng.* **67–68**, 818–825.
25. Bolzon, G., Chiarullo, E. J., Egizabal, P. and Estournes, C. (2010) Constitutive modelling and mechanical characterization of aluminium–based metal matrix composites produced by spark plasma sintering. *Mech. Mater.* **42**, 548–558.
26. Jang, J. I., Choi, Y., Lee, J. S., Lee, Y. H., Kwon, D., Gao, M. and Kania, R. (2005) Application of instrumented indentation technique for enhanced fitness–for–service assessment of pipeline crack. *Int. J. Fract.* **131**, 15–34.
27. Seok, C. S. and Koo, J. M. (2006) Evaluation of material degradation of 1Cr–1Mo–0.25V steel by ball indentation and resistivity. *J. Mater. Sci.* **41**, 1081–1087.
28. EN ISO 6506:2005. Metallic materials – Brinell hardness test.
29. EN ISO 6508:2005. Metallic materials – Rockwell hardness test.
30. ISO 14577: 2002. Metallic materials – Instrumented indentation test for hardness and materials parameters.
31. Bolzon, G. and Buljak, V. (2011) An effective computational tool for parametric studies and identification problems in materials mechanics. *Comp. Mech.* **48**, 675–687.
32. Bolzon, G. and Talassi, M. (2012) Model reduction techniques in computational materials mechanics. In: *Bytes and Science* (G. Zavarise and D. P. Boso, Eds). CIMNE, Barcelona, Spain: 10 pp. in press.
33. Mulford, R., Asaro, R. J. and Sebring, R. J. (2004) Spherical indentation of ductile power law materials. *J. Mater. Res.* **19**, 2641–2649.
34. Jang, J. I., Choi, Y., Lee, Y. H. and Kwon, D. (2005) Instrumented microindentation studies on long-term aged materials: work-hardening exponent and yield ratio as new degradation indicators. *Mater. Sci. Eng., A* **395**, 295–300.
35. ASTM E112 – 10 (2010) Standard test methods for determining average grain size.
36. HKS Inc (2009) *ABAQUS/Standard, Theory and User's Manuals, Release 6.9*. HKS Inc, Pawtucket, RI, USA.
37. The Math Works Inc. (2007) *Matlab, User's Guide and Optimization Toolboxes, Release 7.4.0*. The Math Works Inc, USA.
38. Coleman, T. F. and Li, Y. (1966) An interior trust region approach for nonlinear minimization subject to bounds. *SIAM J. Optim.* **6**, 418–445.
39. Mohanty, S., Chattopadhyay, A., Peralta, P. and Das, S. (2011) Bayesian statistic based multivariate Gaussian process approach for offline/online fatigue crack growth prediction. *Exp. Mech.* **51**, 833–843.
40. Tiago, C. M. and Lietão, V. M. A. (2006) Application of radial basis functions to linear and nonlinear structural analysis problems. *Comput. Math. Appl.* **51**, 1311–1334.
41. Buljak, V. and Maier, G. (2011) Proper Orthogonal Decomposition and Radial Basis Functions in material characterization based on instrumented indentation. *Eng. Struct.* **33**, 492–501.
42. Huber, N., Konstantinidis, A. and Tsakmakis, Ch. (2001) Determination of Poisson's ratio by spherical indentation using Neural Networks. *ASME J. Appl. Mech.* **68**, 218–228.
43. UNI EN ISO 6892-1:2009. Standard: Metallic materials – Tensile testing – Part 1: Method of test at room temperature.

doi: 10.1111/j.1475-1305.2012.00850.x